Supporting Information

Electrochemical surface reconstruction of nickel cobalt pyrophosphate to Ni/Co-hydroxide-(oxy)hydroxide: An efficient and highly durable battery-type supercapacitor electrode material

*Avishek Roy[a], Harish Reddy Inta[a,b], Sourav Ghosh[a], Heramba V. S. R. M. Koppisetti[a], Ayan Mondal[a], Bhagwat Ram Verma[a], Saikat Bag[a], and Venkataramanan Mahalingam[a]**

[a] Department of Chemical Sciences, Indian Institute of Science Education and Research (IISER) Kolkata, Mohanpur, West Bengal 741246, India

[b] Department of Energy Science & Engineering, Daegu Gyeongbuk Institute of Science & Technology (DGIST), Daegu 42988, South Korea

E-mail: mvenkataramanan@yahoo.com

Contents

1.0 Experimental section:

1.1 Materials: cobalt nitrate hexahydrate ($Co(NO_3)_2 \cdot 6H_2O$), ethylene glycol (EG), di ammonium hydrogen phosphate $(NH_4)_2HPO_4$, ammonium chloride (NH_4Cl), Potassium Hydroxide(KOH) were purchased from Merck. Nickel(II) chloride hexahydrate ($NiCl_2 \cdot 6H_2O$) was obtained from Sisco Research Laboratories. Pvt. Ltd. Ethanol (Analytical grade 99%) was purchased from Changshu Hongsheng Fine Chemical Co. Ltd. Polyvinylidene fluoride (PVDF) and Carbon Black (Super P conductive, 99+%) was obtained from Alfa Aesar. Distilled water was used to perform all electrochemical measurements and synthesize all materials. Carbon paper was purchased from the Fuel Cell store. All reagents (analytical grade) were used without further purification.

1.2 Synthesis:

1.2.1 Synthesis of ammonium Cobalt phosphate hydrate (Co_{100} RT):

Co_{100} RT was prepared by a simple Co-precipitation process. Initially, 150mg of $(NH_4)_2HPO_4$ was added to 20 ml distilled water – EG solvent (1:1) and stirred well for 5 mins in a 100ml beaker. Thereafter, in a separate 50ml beaker another 20 ml Water-EG solution (1:1) was prepared and 3g NH_4Cl ammonium chloride followed by 350 mg $Co(NO_3)_2.6H_2O$ were introduced into it. The resultant solution was stirred well for 5 mins. Thereafter the metal precursor solution was dropwise poured into the former phosphate solution and kept stirring for 30mins. The solution was aged (without stirring) for another 30 minutes and allowed the precipitate to settle down. Finally, the obtained pink colour product was centrifuged and washed with distilled water and methanol two times, and dried at 50ºC in a hot air oven for overnight.

1.2.2 Synthesis of ammonium Nickel phosphate hydrate (Ni_{100} RT):

Ni_{100} RT was synthesized using $NiCl_2 \cdot 6H_2O$ precursor via the same method followed in Co_{100} RT synthesis.

1.2.3 Synthesis of Cobalt pyrophosphate (Co_{100} 600) & Nickel pyrophosphate (Ni_{100} 600):

Co_{100} 600 & Ni_{100} 600 were prepared by calcination of Co100 RT & Ni_{100} RT at 600ºC in a Box Furnace with 2º/min ramping rate. The samples were initially soaked for 2 hours under constant heating at 600ºC and allowed to cooled down under 1º/min ramping rate.

1.2.4 Synthesis of Nickel Cobalt pyrophosphate (Ni_xCo_{100-X} 600):

At the beginning, 150mg of $(NH_4)_2HPO_4$ was added to 20 ml distilled water – EG (1:1) solvent and stirred well for 5 mins in a 100ml beaker. Thereafter, in a separate 50ml beaker 20 ml Water-EG (1:1) solvent was taken. Moreover, 3g NH_4Cl followed by 210mg $NiCl_2{\cdot}6H_2O$ (60% of 350mg) & 140mg (40% of 350) $Co(NO_3)_2{\cdot}6H_2O$ (maintain overall metal content 350 mg) were added gradually into the solution and stirred well for 5 mins. Subsequently, the metal precursor solution was dropwise poured into the phosphate solution and kept stirring for 30mins. Next, the solution was aged (without stirring) for another 30 minutes and allowed the precipitate to settle down. Finally, the obtained bluish colour product was centrifuged and washed with distilled water and methanol two times. The blue obtained product was dried at 50ºC in a hot air oven for overnight. The compound is designated as $Ni_{60}Co_{40}$ RT. After that, the sample was calcinated at 600ºC for 2 hours with 2º/min in a box furnace and allowed to cooled down at 1º/min ramping rate. This product is denoted as $Ni_{60}Co_{40}$ 600. For control studies, all the materials were synthesized with different Ni/Co ratio using the same synthesis process and maintaining an overall metal content 350mg. The samples are designated with respect to their Ni/Co ratio and reaction temperature. For instance, (215mg) Ni + (35 mg) Co, (280mg) Ni +(70mg) Co, (245mg) Ni+(105 mg) Co & (175mg Ni) +(175mg) Co are denoted as $Ni_{90}Co_{10}$ 600, Ni_{80}Co20 600, $Ni_{70}Co_{30}$ 600& $Ni_{50}Co_{50}$ 600 respectively.

1.3 Characterization section:

The structural and phase analysis of the materials was performed by x-ray diffractometry (XRD) using a Rigaku miniflex diffractometer with a Cu kα source. The synthesized materials were placed on a quartz glass holder within a diffraction range (2θ) 5 -80° and the spectra were recorded at a scan rate of 5°/min. Again, the XRD of post-electrochemical treatment materials was recorded on a carbon paper substrate at 2°/min scan rate. The Thermogravimetric analysis (TGA) was performed with a PerkinElmer TGA-IR interface TL 8000e instrument with a heating rate 20°/min in a static air atmosphere. Subsequently, the Fourier transform infrared spectroscopy (FTIR) was measured using a PerkinElmer RX1 spectrophotometer equipped with KBr disk technique. The chemical states of the elements present in the as-prepared material, after its precondition and stability were analyzed by an X-ray photoelectron spectrometer (XPS, PHI 5000 Versa Probe II, ULVAC-PHI Inc., USA) equipped with micro-focused (100 μm, 15 kV) monochromatic Al-Kα X-Ray source (hν = 1486.6 eV). The survey scans were recorded using an X-ray source power of 50W with a pass energy of 187.85 eV. High-

resolution spectra of the individual elements were measured at 46.95 eV pass energy. The measured XPS raw data were fitted using Casa XPS software. Further, the Surface characteristics and porosity of the materials were analyzed by a multi-point BET analyser (QuadraSorb Station 2). To investigate the morphology of the as-synthesized materials, after preconditioning and stability test Field emission scanning emission microscopy (FESEM, ZEISS SUPRA 55-VP JSM equipped with EDAX of GEMINI column technology) and High-Resolution Transmission electron microscope (HRTEM) (JEOL, JEM-2100F) was performed. For FESEM and HRTEM measurements the samples are initially well dispersed in methanol and drop casted on a silicon wafer and Copper grid, respectively. After that, the drop casted Copper grid was drying well under vacuum. To probe the etching of pyrophosphate moieties ICP-AES analysis was performed using SPECTRO Analytical Instruments. For the electrochemical measurements, All the materials drop casted on a carbon paper substrate (in an area of 0.5 cm X 0.5 cm both side). All the electrochemical data was recorded by biologic SP300 workstation.

1.4 Electrochemical measurement:

The electrochemical measurements were performed in a three-electrode setup using 1M KOH as electrolyte. Herein, Ag/AgCl (3.5M KCl) & Pt wire are used as reference and counter electrode, respectively. Further, the working electrode was prepared by the drop-casting method. Using 8mg of as prepared $Ni_{60}Co_{40}$ 600 sample followed by 1 mg PVDF (as a polymeric binder) and 1 mg Carbon black. The mixture was well grinded with a mortar pestle using 200 µL ethanol and dried well at room temp. This process was carried out total of three times sequentially to obtain a fine homogenous mixture. Thereafter, 2mg of resulted mixture was dispersed in 240 µL ethanol in an eppendorf viol followed by ultra-sonication for 15 min. Finally, the dispersed solution was considered as ink, and 30 µL (twice each side) of dispersion as total 120 µL was drop-casted onto a carbon paper in an area of $0.5*0.5cm^{-2}$. So, the total catalyst loading is 1mg. Subsequently, the Cyclic voltammetry (CV) technique was performed for electrochemical activation of electrode materials within the voltage window of 0 - 0.65V vs Ag/AgCl. For activation of electrode material 200 CV cycles were conducted at 50 mV/s scan rate. Further CV was performed at different scan rates from 5 to 50 mV/s in the same voltage window. The Galvanostatic charge-discharge (GCD) estimation was conducted with varying current densities from 1 to 20 Ag^{-1}. The electrochemical impedance spectroscopy (EIS) technique was executed using AC voltage, with a frequency range of 200 kHz to 0.01 Hz at open circuit potential (OCP) (E = 0.0 V).

The specific Capacitance (C_{sp}) (Fg^{-1}) as well as specific capacity (C_s) (Cg^{-1}) was measured from both CV and GCD techniques. From CV curve C_{sp} and C_s was calculated by using the following mathematical formula (Equation 1 & 2)

$$C_{sp} = \frac{\int I\,(V)dV}{2m\,\Delta V\,(\frac{dV}{dt})} \quad \text{----------} \quad (1)$$

$$C_s = \frac{\int I\,(V)\,dV}{2m\,(\frac{dV}{dt})} \quad \text{----------} \quad (2)$$

Where, ∫ I (V) dV denotes integrated CV area, (dV/dt) as CV scan rate (mVs^{-1}), I is associated to the discharge current (A), m is the total mass of as prepared ink loaded in the working electrode (mg), & ΔV, Δt designates operational voltage window (V) and discharge time (Sec) of the electrode material, respectively.

Further, the $C_{sp}$and C_s were calculated by GCD techniques with the mathematical formula Shown below (Equations 3 & 4)

$$C_{sp} = \frac{I\Delta t}{m\Delta V} \quad \text{----------} \quad (3)$$

$$C_s = \frac{I\Delta t}{m} \quad \text{----------} \quad (4)$$

Here, I denotes the current (A) used to perform the GCD test.

1.5 Hybrid Device Construction:

A hybrid device was constructed using two electrodes set up. Herein, activated charcoal (AC) and electrochemically activated $Ni_{60}Co_{40}$ 600 material are considered as negative and positive electrodes respectively. The final mass loading of the electrodes was optimized by the charge mass balance equation following (Equation 5)

$$m+/m- = C+V+ / C-V- \quad \text{----------} \quad (5)$$

Where, m+, m- are the mass loading, C+, C- are specific capacitance (Fg^{-1}) & V+, V- are the individual operational voltage window of the positive and negative electrodes, respectively. The independent voltage window of activated $Ni_{60}Co_{40}$ 600 and AC are 0.45 V and 1 V,

respectively. The calculated specific capacitance values of activated $Ni_{60}Co_{40}$ 600 and AC are 566 Fg^{-1} and 83 Fg^{-1} at 1Ag^{-1} current density. Hence, to construct the hybrid device, the final mass loading of $Ni_{60}Co_{40}$ 600 and AC are approximately 1mg (4 mg cm^{-2}) and 3mg (12 mg cm^{-2}), and thus the m+/m- ratio is maintained as 1:3.

The energy density (E) & Power density (P) of the hybrid device were measured by following the mathematical formula (Eq. 6 & 7 respectively)

$$E = \frac{Csp\,\Delta V^2}{2}\,\frac{1000}{3600} \quad \text{----------(6)}$$

$$P = \frac{E}{\Delta t}\,3600 \quad \text{---------- (7)}$$

Where Csp denotes specific capacitance (Fg^{-1}), ΔV is the operational voltage window, and Δt is the discharge time of the hybrid Capacitor. E, P indicate energy density ($Whkg^{-1}$) and power density (Wkg^{-1}), respectively.

Electrolyte Optimization:

To understand the optimal electrolyte concentration of $Ni_{60}Co_{40}$ 600, initial electrochemical activation was performed using the CV technique (50 mV/s) in 0.5M, 1M, and 2M KOH electrolytes. Subsequently, the resultant materials are subjected to CV (at 5 mV/s) and GCD test (1 Ag^{-1} current density) for the determination of optimum electrolyte concentration (*Vide infra*).

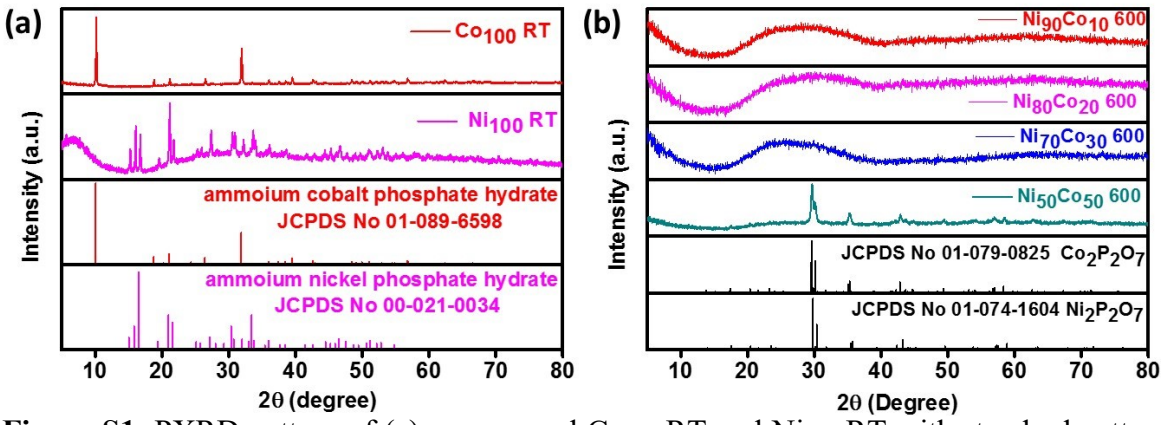

Figure S1: PXRD pattern of (a) as prepared Co_{100} RT and Ni_{100} RT with standard pattern of ammonium nickel phosphate hydrate (JCPDS No # 00-021-0034), and ammonium cobalt phosphate hydrate, respectively (JCPDS No # 01-089-6598), (b) as prepared $Ni_{90}Co_{10}$ 600,

$Ni_{80}Co_{20}$ 600, $Ni_{70}Co_{30}$ 600, $Ni_{50}Co_{50}$ 600 with standard pattern of $Ni_2P_2O_7$ (JCPDS No # 01-074-1604) & $Co_2P_2O_7$ (JCPDS No # 01-079-0825).

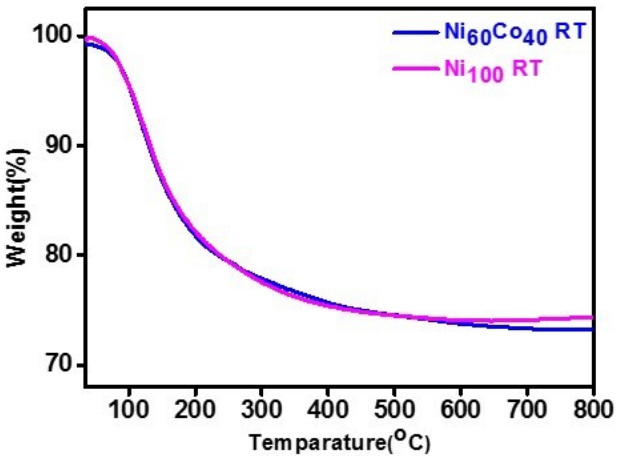

Figure S2: TGA analysis of Ni_{100} RT and $Ni_{60}Co_{40}$ RT

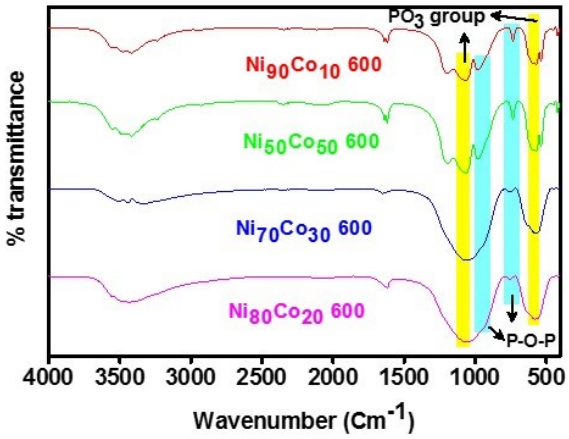

Figure S3: FTIR spectra of as prepared $Ni_{90}Co_{10}$ 600, $Ni_{80}Co_{20}$ 600, $Ni_{70}Co_{30}$ 600, $Ni_{50}Co_{50}$ 600 samples.

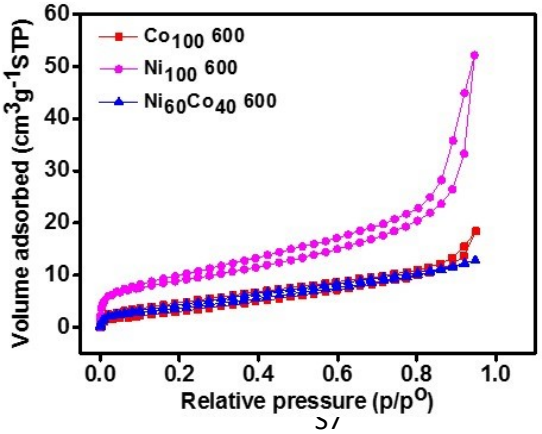

Figure S4: Nitrogen adsorption-desorption isotherm of as-prepared Ni_{100} 600, Co_{100} 600 and $Ni_{60}Co_{40}$ 600

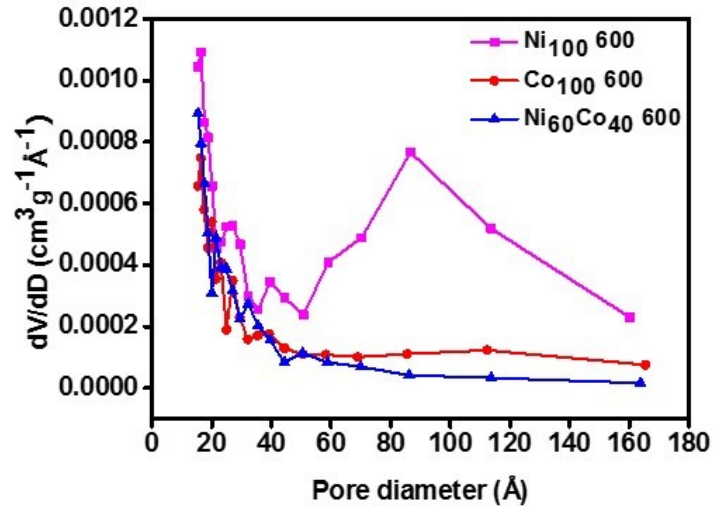

Figure S5: BJH Pore Width distribution measurement of as prepared samples Ni_{100} 600, Co_{100} 600, $Ni_{60}Co_{40}$ 600

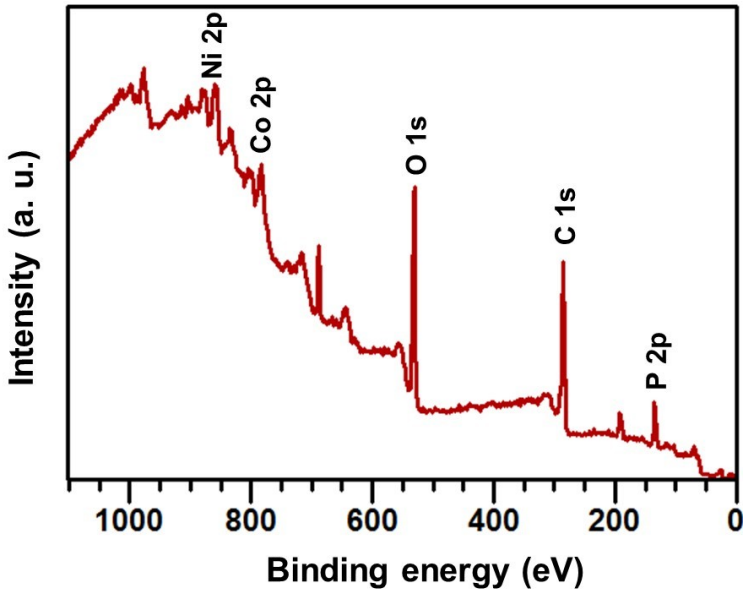

Figure S6: X-ray photoelectron spectroscopy (XPS) survey scan of as-prepared $Ni_{60}Co_{40}$ 600 sample.

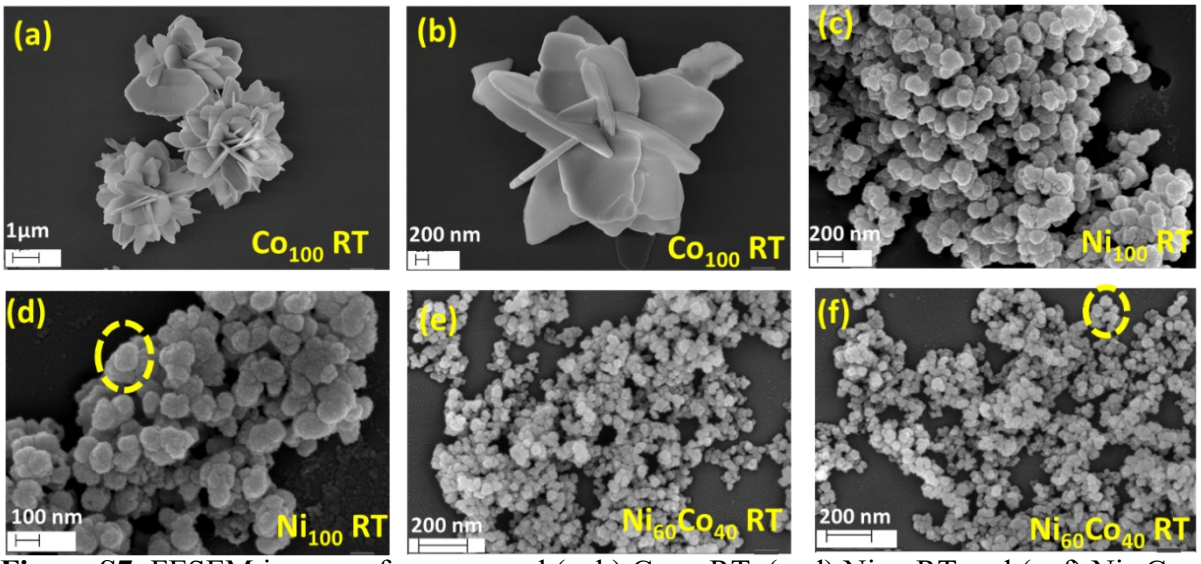

Figure S7: FESEM images of as-prepared (a, b) Co_{100} RT, (c, d) Ni_{100} RT and (e, f) $Ni_{60}Co_{40}$ RT

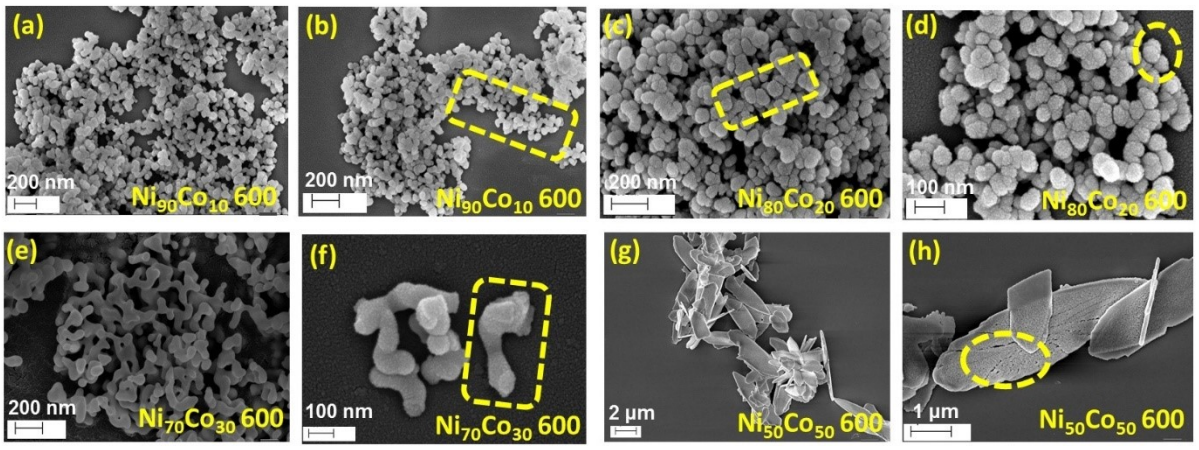

Figure S8: FESEM images of as prepared (a, b) $Ni_{90}Co_{10}$ 600, (c, d) $Ni_{80}Co_{20}$ 600, (e, f) $Ni_{70}Co_{30}$ 600, and (g, h) $Ni_{50}Co_{50}$ 600

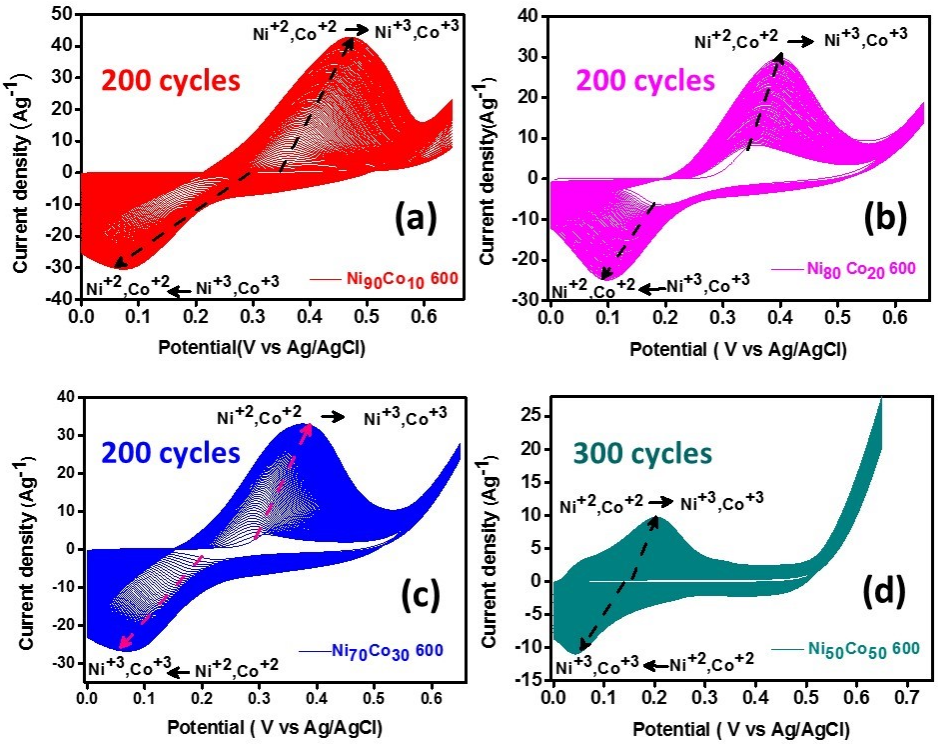

Figure S9: Cyclic voltammetry curves up to 200 cycles for (a) $Ni_{90}Co_{10}$ 600, (b) $Ni_{80}Co_{20}$ 600, (c) $Ni_{70}Co_{30}$ 600 and (d) 300 cycles for $Ni_{50}Co_{50}$ 600 recorded in 1M KOH

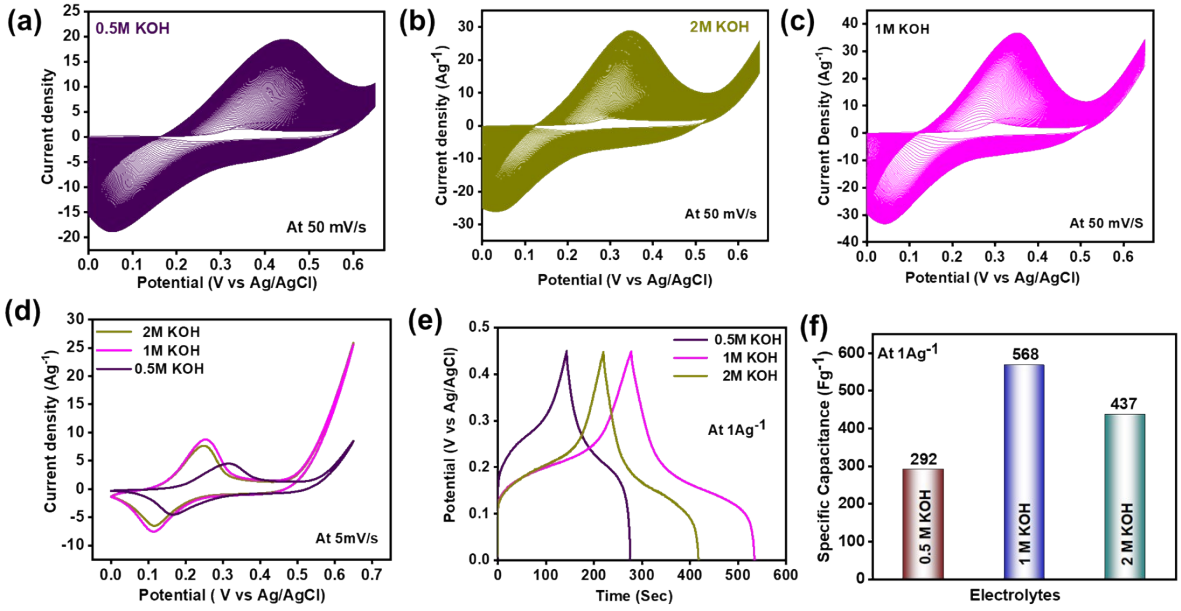

Figure S10: (a-c) CV curves at 50mV/s scan rates, (b) CV curves at 5 mV/s scan rate (c) GCD curves at 1Ag^{-1} current density, and (d) bar diagram represents the corresponding specific

capacitance values (obtained from GCD curves) of $Ni_{60}Co_{40}$ 600 in different KOH electrolytes (0.5M, 1M, and 2M).

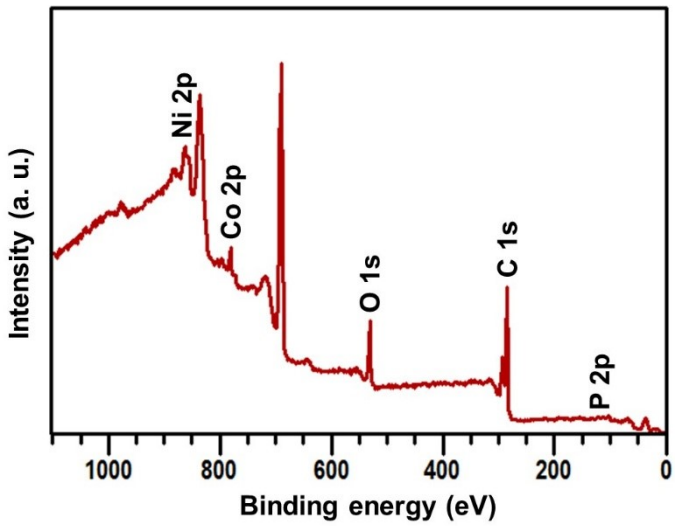

Figure S11: X-ray photoelectron spectroscopy (XPS) survey scan of $Ni_{60}Co_{40}$ 600 after electrochemical preconditioning (after 200 cycles).

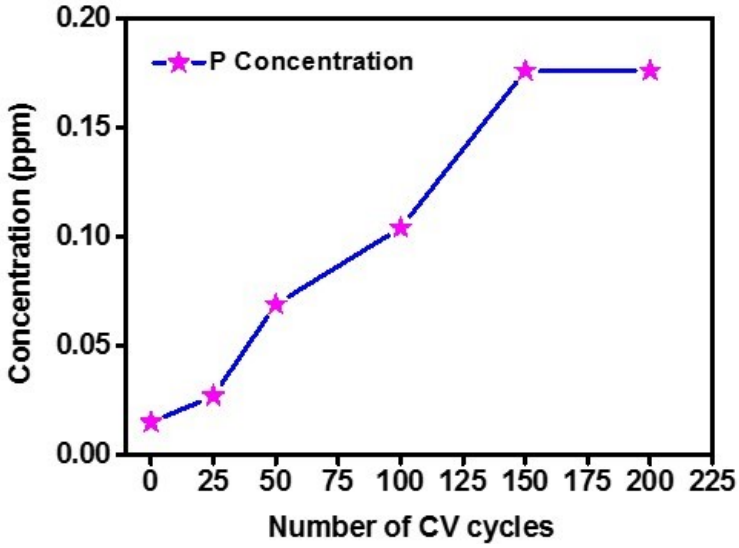

Figure S12: ICP-AES analysis of the electrolyte collected after different cycles of electrochemical precondition (activation process) for $Ni_{60}Co_{40}$ 600.

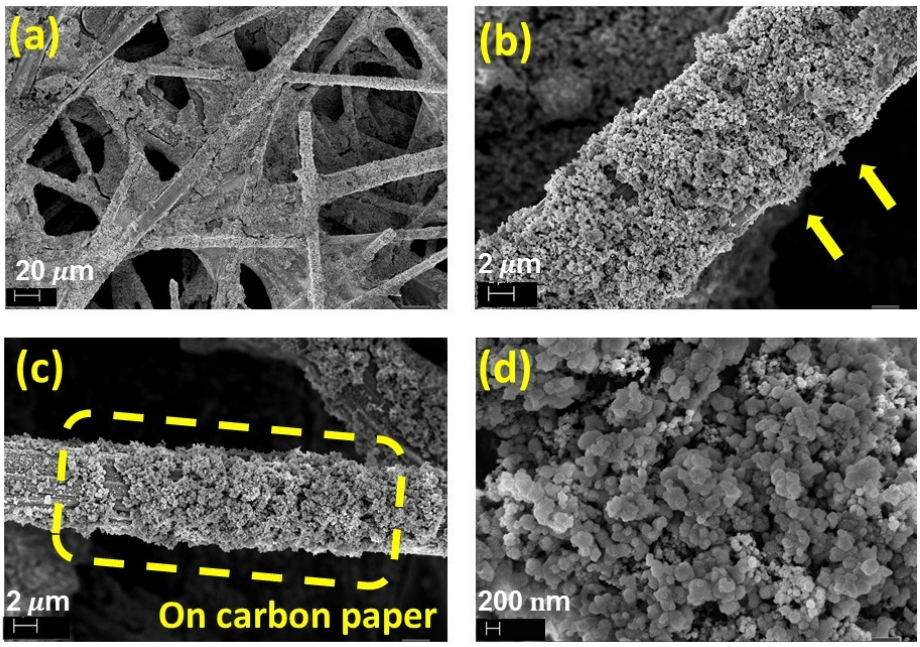

Figure S13: FESEM images of (a - d) electrochemically activated $Ni_{60}Co_{40}$ 600 (on carbon paper substrate).

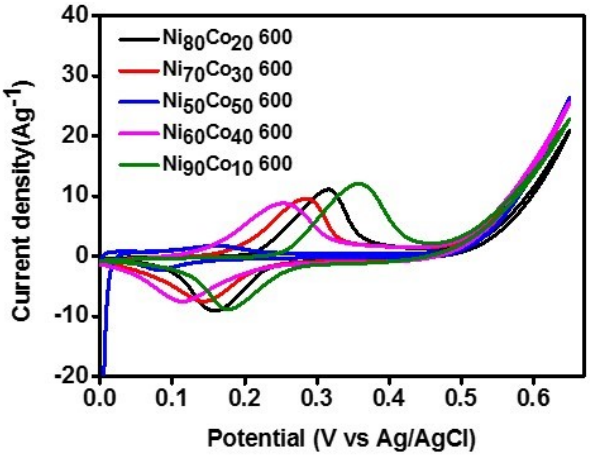

Figure S14: Cyclic Voltammograms of as-prepared materials with different compositions of Ni/Co ratio measured at 5 mV/S scan rate in 1M KOH.

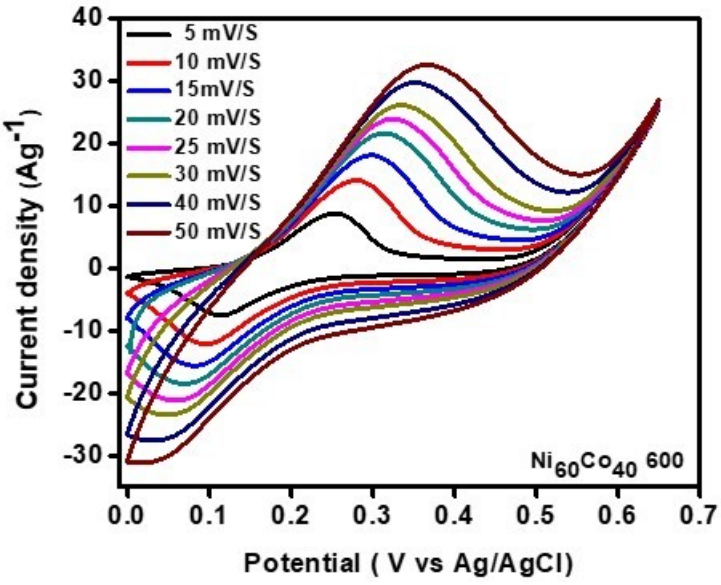

Figure S15: Cyclic voltammetry curves of $Ni_{60}Co_{40}$ 600 with varying scan rates (5-50 mV/s) in 1M KOH

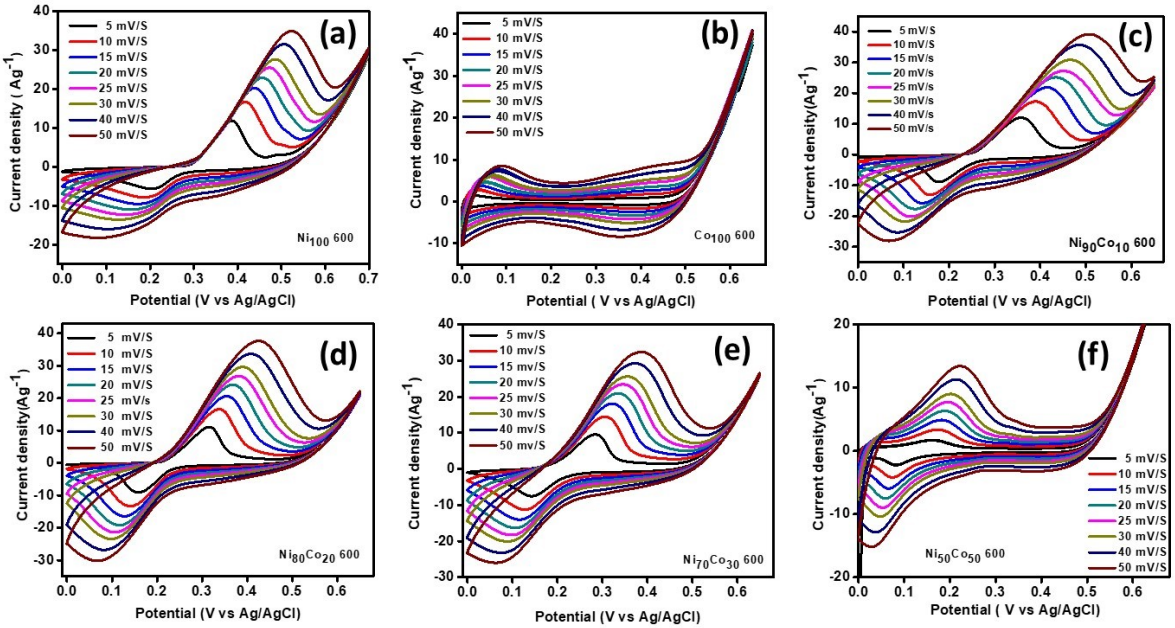

Figure S16: Cyclic voltammetry curves for (a) Ni_{100} 600 (b) Co_{100} 600 (c) $Ni_{90}Co_{10}$ 600 (d) $Ni_{80}Co_{20}$ 600 (e) $Ni_{70}Co_{30}$ 600 and (f) $Ni_{50}Co_{50}$ 600 recorded with varying scan rates (5-50 mV/s) in 1M KOH.

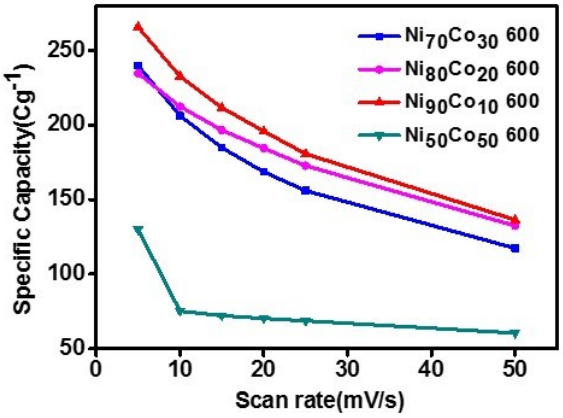

Figure S17: Graph of Variation of specific capacity vs. scan rate plot for electrochemically activated $Ni_{90}Co_{10}$ 600, $Ni_{80}Co_{20}$ 600, $Ni_{70}Co_{30}$ 600, and $Ni_{50}Co_{50}$ 600 recorded in 1M KOH

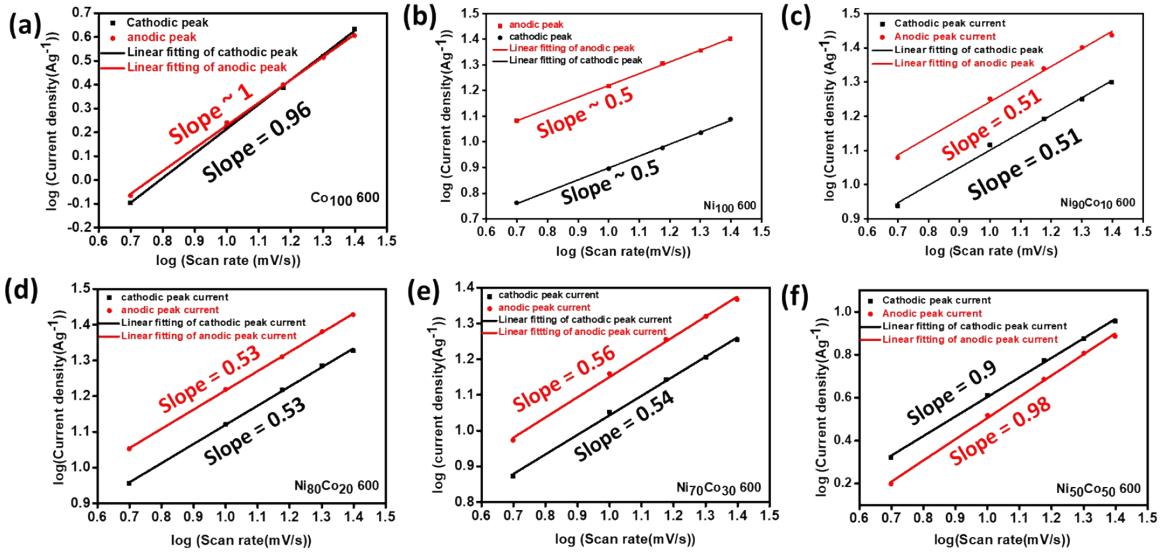

Figure S18: Estimation of b values for electrochemically activated (a) Co_{100} 600, (b) Ni_{100} 600, (c)$Ni_{90}Co_{10}$ 600, (d) $Ni_{80}Co_{20}$ 600, (e) $Ni_{70}Co_{30}$ 600, and (f)$Ni_{50}Co_{50}$ 600. from both anodic and cathodic peak currents.

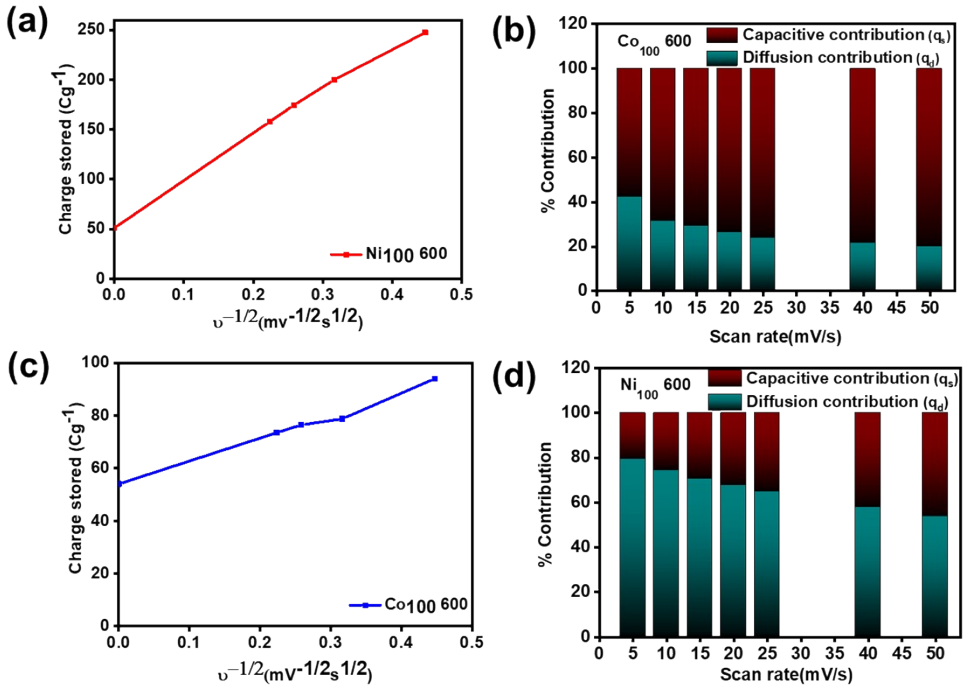

Figure S19: The plot of specific capacity (Cg^{-1}) Vs the inverse of the square root of scan rate (υ) for (a) Ni_{100} 600, (c) Co_{100} 600. The (b, d) is representing the bar diagram for % of capacitive and diffusion contribution with respect to the total charge storage for Ni_{100} 600, Co_{100} 600, respectively.

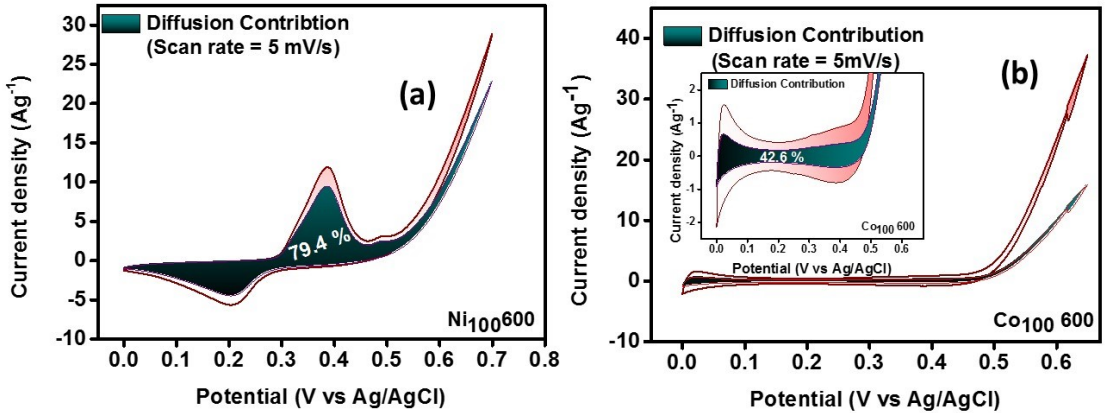

Figure S20: The individual diffusion or Capacitive contribution in the entire charge storage of electrochemically activated (a) Ni_{100} 600 (b) Co_{100} 600 measured at 5 mV/s Scan rate. The dark green colour region represents the diffusion contribution in the particular scan rate. (Inset of

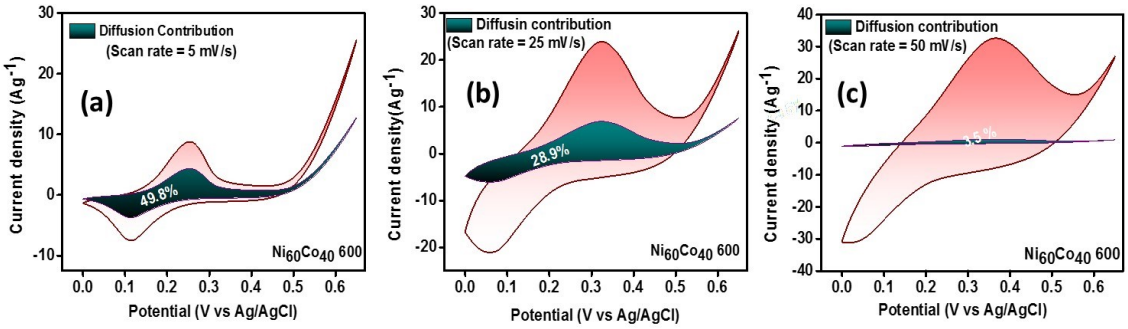

Figure S21: The individual diffusion and capacitive contributions towards the total charge storage ability of activated $Ni_{60}Co_{40}$ 600 with varying scan rates (a) 5 mV/s (b) 25 mV/s and (c) 50 mV/s. The dark green colour region represents only the diffusion contribution.

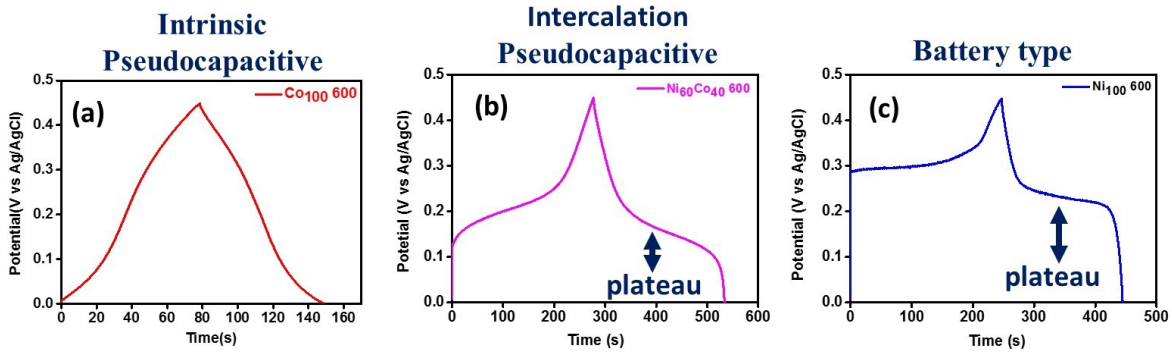

Figure S22: GCD curves represent different charge storage behaviour of (a) Co_{100} 600, (b) $Ni_{60}Co_{40}$ 600, and (c) Ni_{100} 600 recorded at $1Ag^{-1}$ current density in 1M KOH.

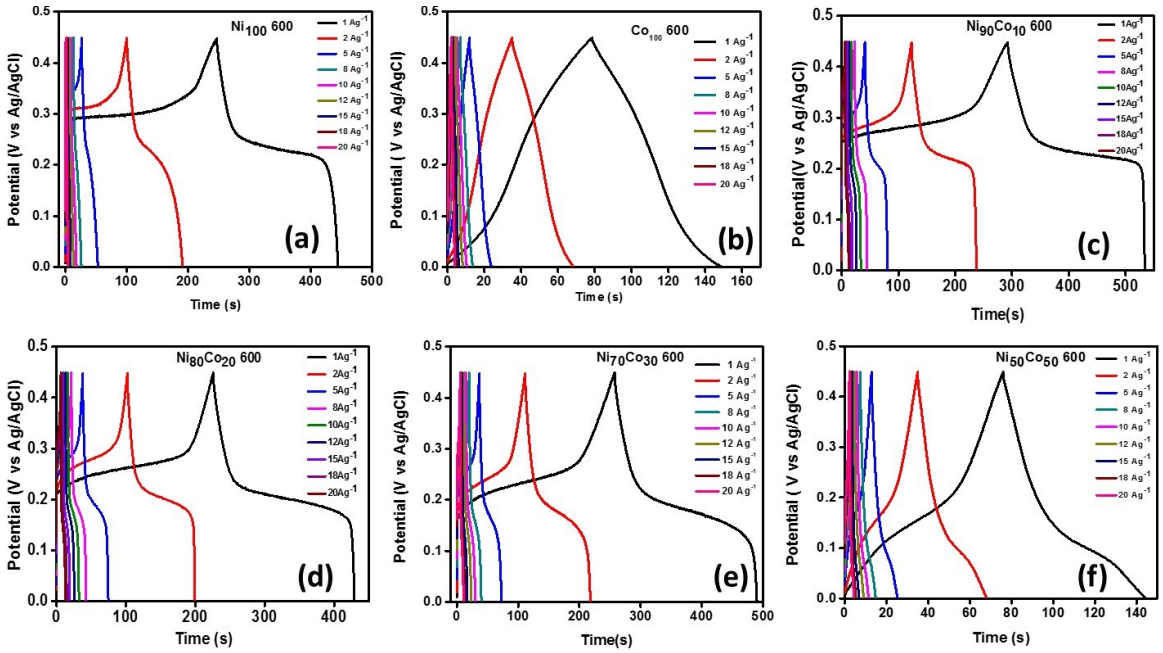

Figure S23: GCD curves of electrochemically activated (a)Ni_{100} 600 (b) Co_{100} 600 (c) $Ni_{90}Co_{10}$ 600 (d)$Ni_{80}Co_{20}$ 600 (e) $Ni_{70}Co_{30}$ 600 and (f) $Ni_{50}Co_{50}$ 600 recorded at different current densities (1 to 20 Ag^{-1}) at 1M KOH electrolyte.

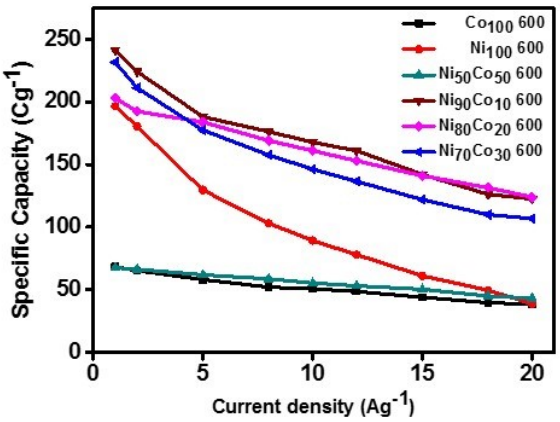

Figure S24: Specific Capacity vs. Current density plot for activated Ni_{100}600, Co_{100} 600, $Ni_{90}Co_{10}$ 600, $Ni_{80}Co_{20}$ 600, $Ni_{70}Co_{30}$ 600 and $Ni_{50}Co_{50}$ 600.

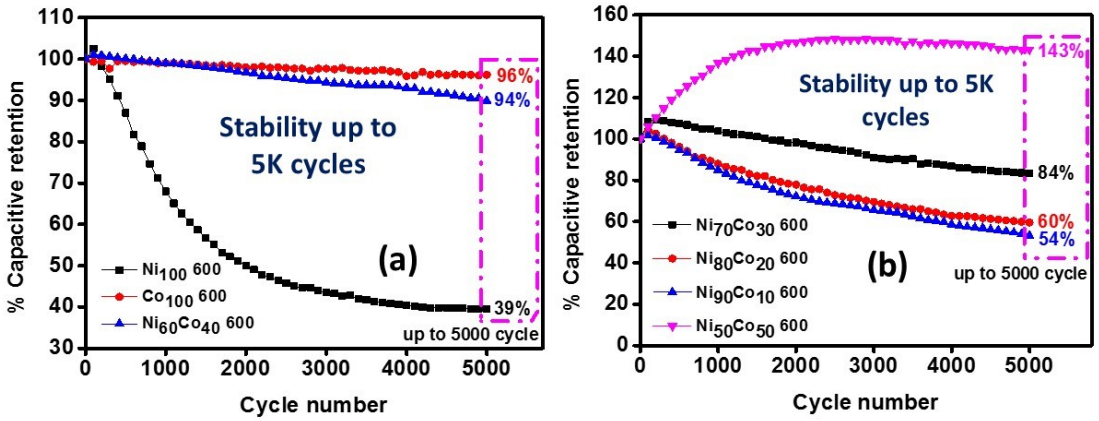

Figure S25: Cyclic stability plot of electrochemically activated (a) Ni_{100} 600, Co_{100} 600, and $Ni_{60}Co_{40}$ 600 (b) Activated materials with different compositions of Ni/Co ratio obtained at current density 10 Ag^{-1} (up to 5000 cycles in A three electrode system).

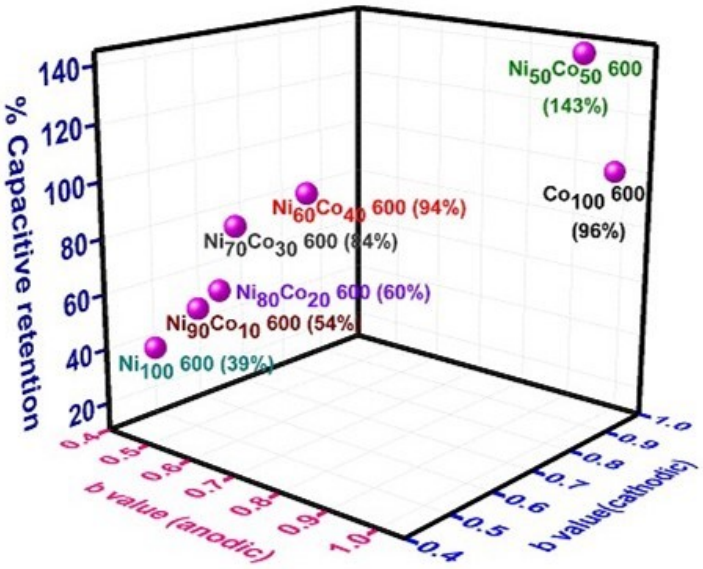

Figure S26: 3D Scatter plot of b value (from cathodic & anodic peak currents) and % capacitive contribution (up to 5000 cycles at 10 Ag^{-1} current density) for all electrochemically activated materials.

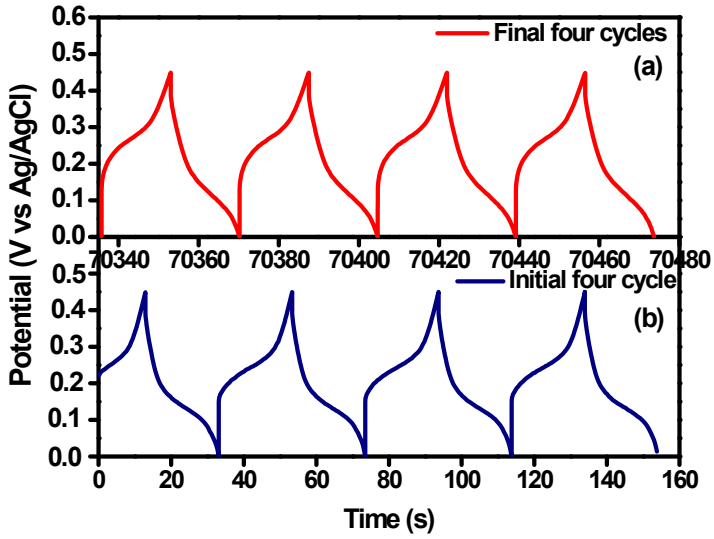

Figure S27: GCD curves of activated $Ni_{60}Co_{40}$ 600 at $10Ag^{-1}$ for (a) initial and (b) final four cycles (at10000 cycles) of stability experiment in a three-electrode system (in 1M KOH).

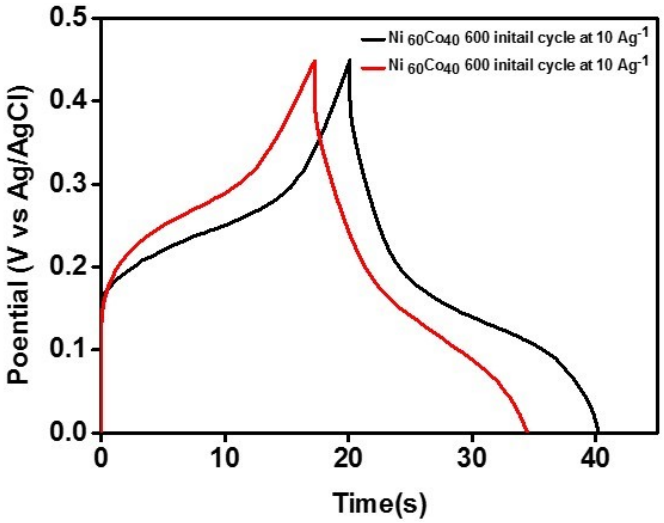

Figure S28: GCD curves of activated $Ni_{60}Co_{40}600$ recorded at 10 Ag^{-1} before and after stability experiment in three electrode system.

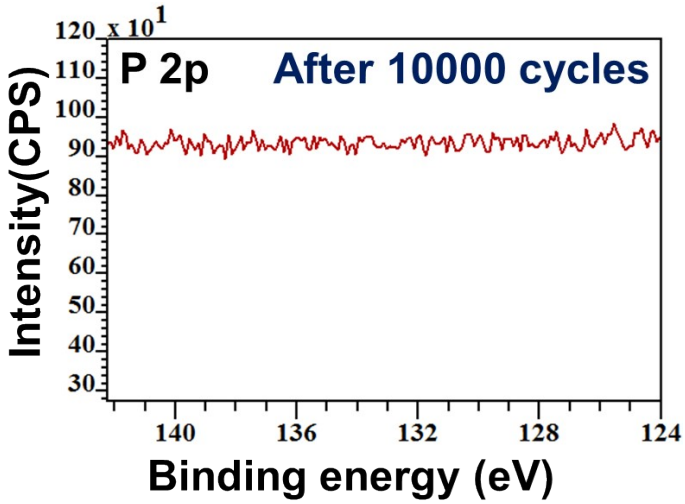

Figure S29: High resolution XPS spectrum of activated $Ni_{60}Co_{40}$ 600 after electrochemical stability (up to 10000 cycles) in 1M KOH.

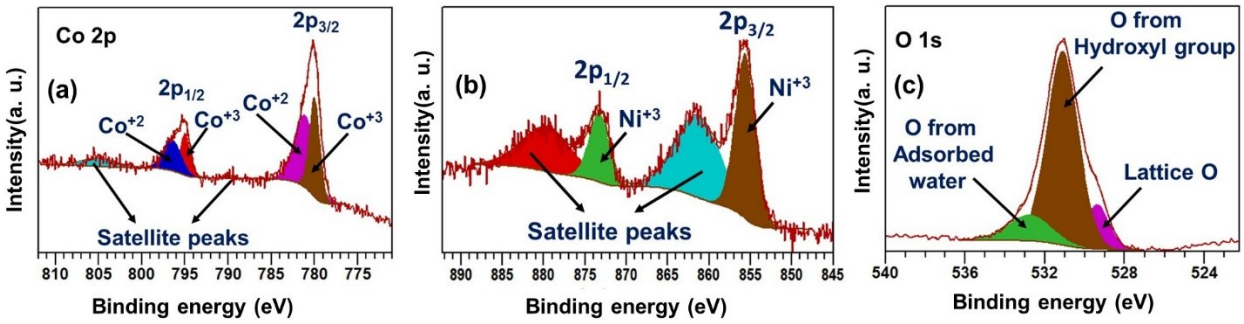

Figure S30: High resolution X-ray photoelectron spectroscopy of (a) Co 2p, (b) Ni 2p (c) O 1s after electrochemical stability test.

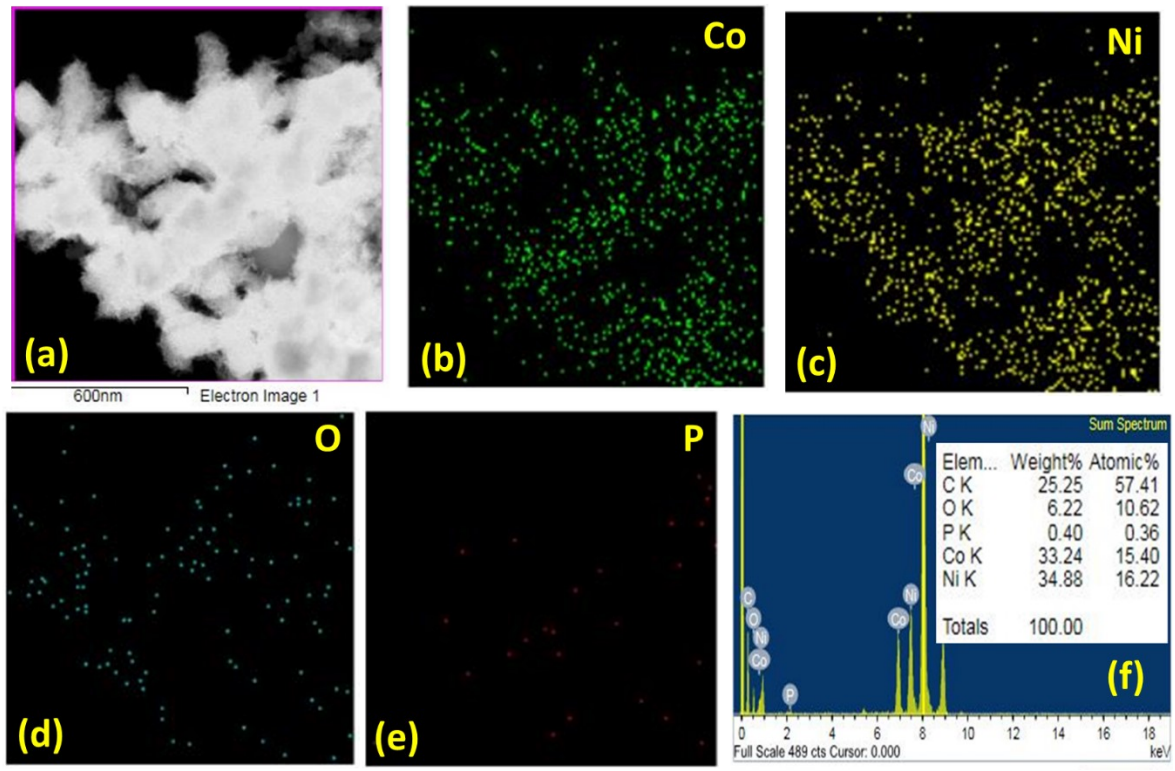

Figure S31: (a-e) Elemental mapping, (f) EDS analysis of Co, Ni, O, P for activated $Ni_{60}Co_{40}$ 600 after the electrochemical stability test (10000 cycles).

Synthesis of Ni, Co hydroxide:

Herein, we have taken an isotropic quantity of $NiCl_2 \cdot 6H_2O$ and $Co(NO_3)_2 \cdot 6H_2O$ salts (60 : 40) used in $Ni_{60}Co_{40}$ 600 synthesis and dissolved in 30 ml H_2O. Subsequently, 10ml of aqueous NH_3 (1:1) was dropwise introduced into the solution and stirred for 3 hours. The resultant solution turned green, centrifuged, and dried under vacuum.

Physical Characterization of Ni, Co hydroxide:

To understand the phase of the as-synthesized material, PXRD analysis was performed. The PXRD patterns of the as-prepared material closely matched with the standard pattern of $Ni(OH)_2$ (ICDD No: 38-0715) and $Co(OH)_2$ (ICDD No: 46-0605) and thereby confirm the formation of Ni, Co hydroxide **(Figure S32a)**. Subsequently, the XPS study was performed to understand the chemical state of the elements in the materials. The XPS survey scan reveals

the presence of Ni, Co, and O in the material **(Figure S32b)**. Further, the deconvolution of individual high-resolution Ni and Co 2p spectra confirms the presence of Ni^{+2} and Co^{+2}, respectively **(Figure S32c, d)**. In addition, the peak-fitted O 1s scan manifests the presence of a hydroxyl group in the as-prepared material **(Figure S32e)**. These consequences mentioned above strongly support the formation of Ni,Co hydroxide.

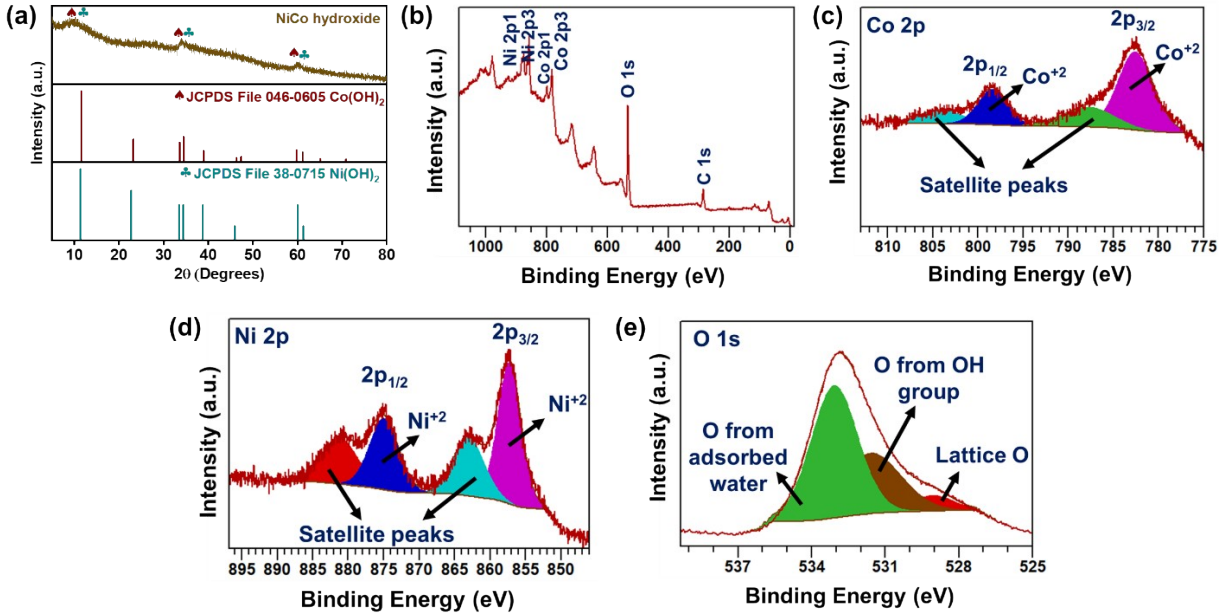

Figure S32: (a) PXRD analysis, (b) XPS survey scan, high-resolution XPS scan (c) Co 2p, (d) Ni 2p, and (e) O 1s for as-prepared Ni, Co hydroxide

Morphological characterization:

The surface textural patterns of as-prepared Ni, Co hydroxide was confirmed by TEM analysis. The TEM images display a flake-like microstructure of Ni, Co Hydroxide **(Figure S33(a-c))**. On the other hand, the EDS study and elemental mapping analysis confirm the presence of Ni, Co and their uniform distribution in the Ni, Co hydroxide material **(Figure S33(d-h))**.

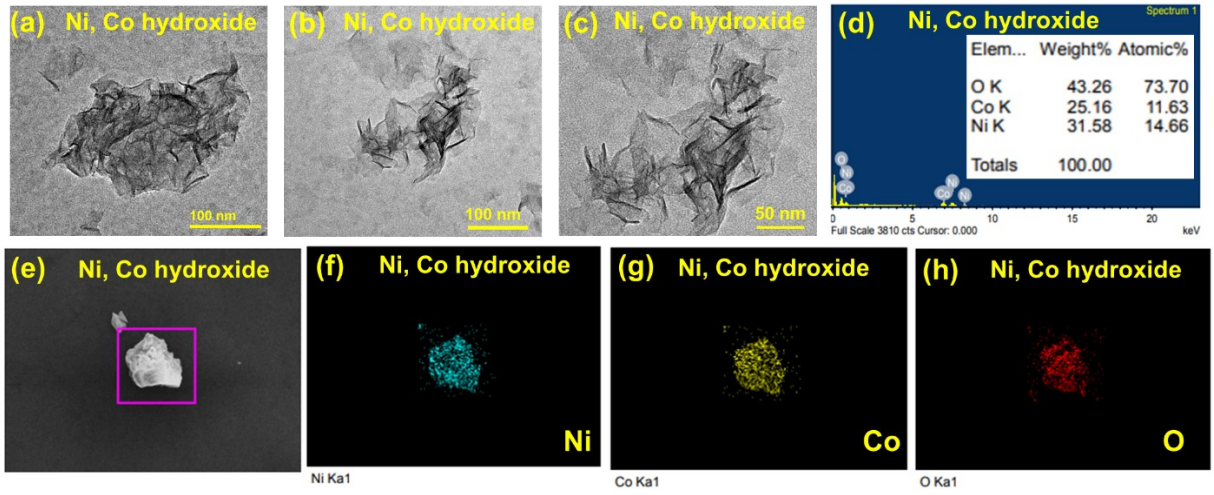

Figure S33: (a-c) TEM images, (d) EDS study, (e-f) elemental mapping of as-prepared Ni, Co hydroxide

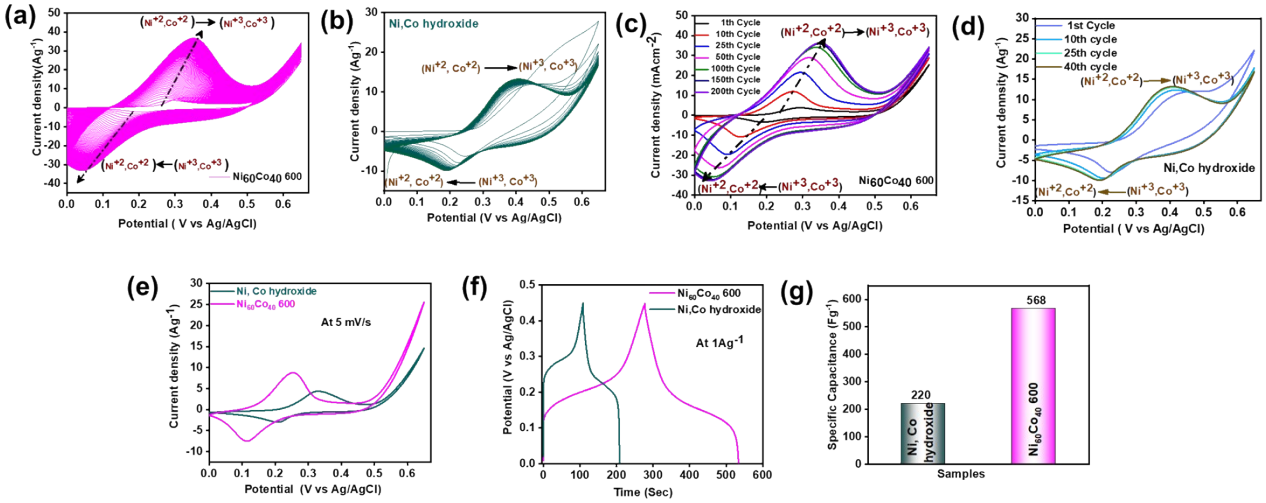

Figure S34: (a, b) CV curves representing the continuous improvement in redox current density during preconditioning, (c, d) Comparison of redox current density, Comparison of (e) CV curves (at 5mV/s), (f) GCD curves ($1Ag^{-1}$) between $Ni_{60}Co_{40}$ 600 and Ni, Co hydroxide, respectively (g) bar diagram representing specific capacitance values obtained from GCD curves

Etching mechanism of Pyrophosphate:

There are two controlling factors that guide the etching process. (a) breakdown of pyrophosphate (diphosphate) to monophosphate, and (b) high solubility of potassium phosphate in alkaline conditions.

In pyrophosphate ($P_2O_7^{4-}$), two PO_4^{3-} units are interconnected through the P-O-P unit. Therefore, pyrophosphates are also designated as diphosphate. Under strong alkaline conditions (pH=14) the pyrophosphate breaks down and is converted to phosphate units.

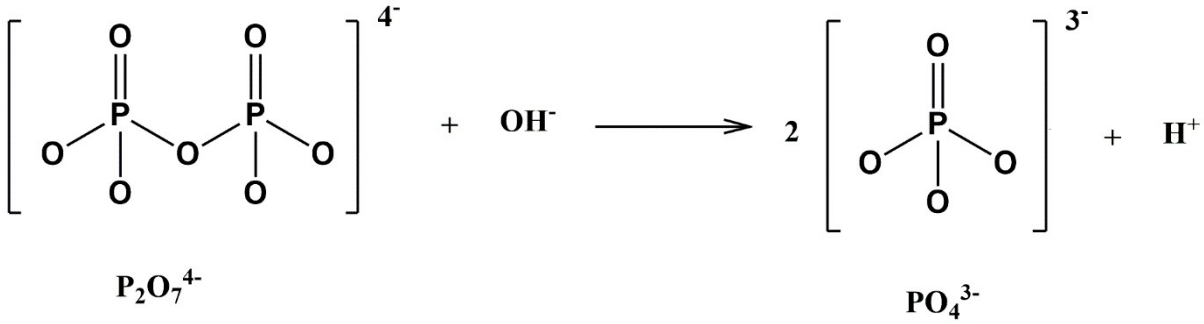

According to the Pourbaix diagram of phosphorus, the PO_4^{3-} units can exist at pH 14.[1] As, the electrochemical study was performed at pH 14, the pyrophosphate or diphosphate units first dissociate into a monophosphate structure. Further, the oxidation of metals (Ni, Co) disturbs the local environment around the phosphate moieties and this is likely to help the interaction with K^+ (from the KOH electrolyte). As a result, the anion exchange occurs between PO_4^{3-} and OH^- leading to the surface reconstruction process. Therefore, the binding site is critically disordered under the experimental conditions that correspond to the leaching of phosphate moieties into the electrolyte solution and transformed into hydroxide/ (oxy) hydroxide species. Based on the above-mentioned supports the plausible reaction mechanism could be as follows:

$$Ni_{60}Co_{40}\ 600 \sim Ni,Co\ pyrophosphate \sim Ni,Co\ P_2O_7$$

$$Ni,Co\ P_2O_7 \rightarrow Ni,Co\ PO_4\ (\text{In 1M KOH medium pH 14}) \text{ ----------(8)}$$

$$Ni,Co\ PO_4 + OH^- \rightarrow Ni,Co\ (OH)_2 + PO_4^{3-} + H_2O + e^-\ \text{(Formation of hydroxide species)---(9)}$$

$$Ni,Co\ (OH)_2 + OH^- \rightarrow Ni,Co\ (OOH) + H_2O + e^-\ \text{(Formation of (oxy)hydroxide species)--(10)}$$

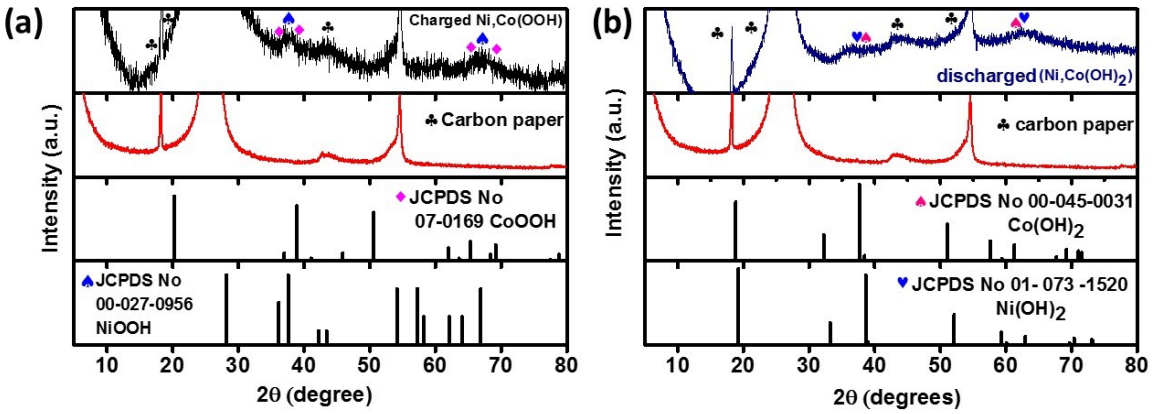

Figure S35: PXRD patterns of activated $Ni_{60}Co_{40}$ 600 electrode material recorded at **(a)** charged, **(b)** discharged states along with standard patterns of CoOOH (JCPDS # 07-0169), NiOOH (JCPDS # 00-027-0956), $Co(OH)_2$ (JCPDS # 00-045-0031), $Ni(OH)_2$ (JCPDS # 073-1520)

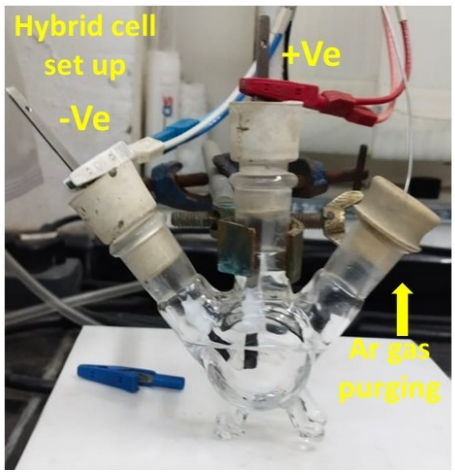

Figure S36: Digital image of the two-electrode set up used for the measurement of $Ni_{60}Co_{40}$ 600//AC hybrid device.

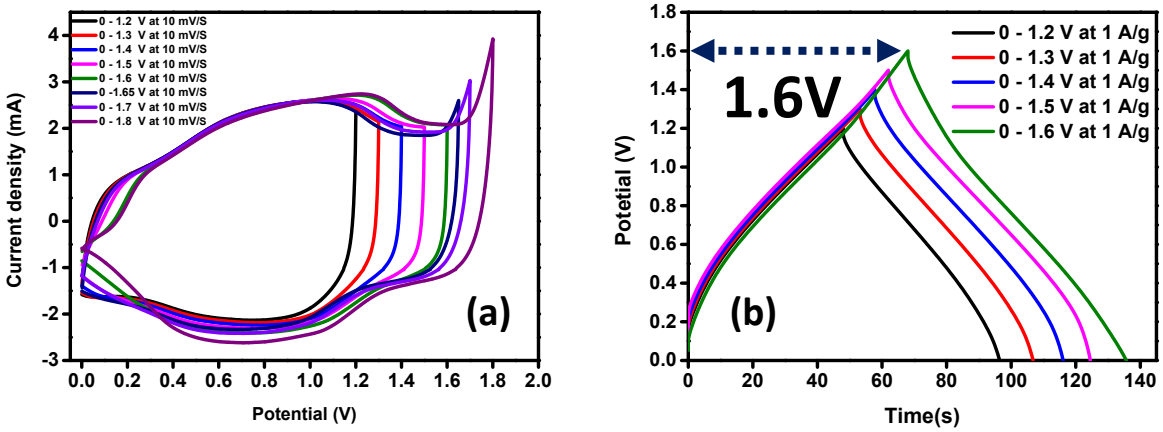

Fig S37: (a) CV profiles (at a constant scan rate of 10 mVs^{-1}) in 1.2 to 1.8 V voltage window (b) GCD curves (at constant 1 Ag^{-1}current density) of AC// $Ni_{60}Co_{40}$ 600 hybrid capacitor recorded at different voltage windows.

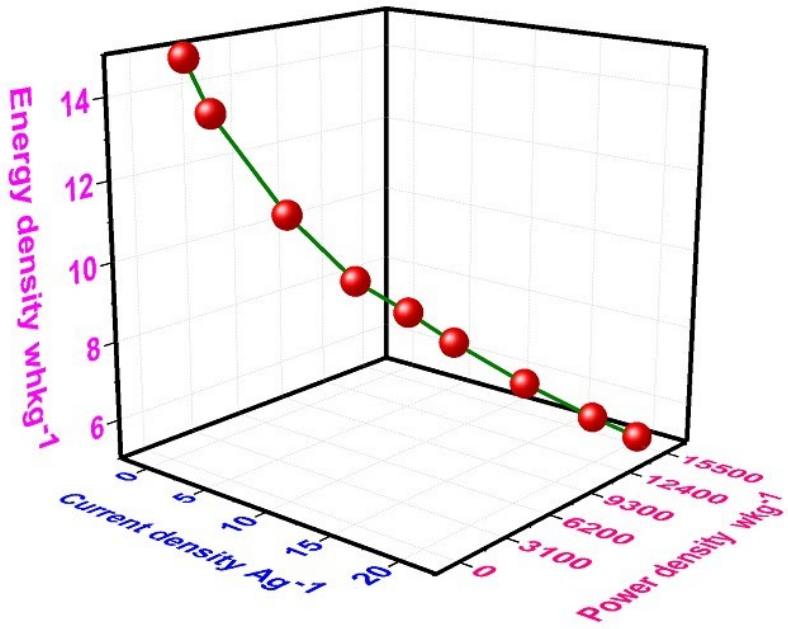

Figure S38: 3D Scatter plot showing the correlation of current density (1 to 20Ag^{-1}) with corresponding power density and energy density of $Ni_{60}Co_{40}$600 //AC hybrid device.

Table S1: Porosity and Surface area study of as-prepared pyrophosphate samples.

SL No	Sample Id	S_{BET} (m^2/g)	$V_{P\text{-}Total}$ (cc/g)	Pore Diameter (nm)
1.	Ni_{100} 600	32	0.073	7.6
2.	Co_{100} 600	12	0.024	2.1
3.	$Ni_{60}Co_{40}$ 600	14	0.015	2.2

Table S2: ICP-AES analysis of Nickel (Ni), Cobalt (Co) in the as prepared $Ni_{60}Co_{40}$ 600.

Sample	Theoretical ratio of Ni & Co		Experimental ratio of Ni & Co (analysed by ICP-AES)	
$Ni_{60}Co_{40}$ 600	0.60 (Ni)	0.40 (Co)	0.52 (Ni)	0.48 (Co)

Table S3: The Cobalt (Co), Nickel (Ni) and phosphorous (P) concentrations in the electrolyte obtained from ICP-AES analysis.

 # ND = not detected (means less than 0.01ppm)

CV cycle number	Cobalt (Co) amount (ppm)	Nickel (Ni) amount (ppm)	Phosphorous (P) amount (ppm)
0	ND	ND	0.015
25	ND	ND	0.027
50	ND	ND	0.069
100	ND	ND	0.104
150	ND	ND	0.176
200	ND	ND	0.176

Table S4: The cyclic stability and specific capacitance results of all the electrochemically activated pyrophosphate materials in three electrode system (in 1M KOH).

Sample id	Capacitance (Fg^{-1})	Stability (%) (5000 cycle) (at $10Ag^{-1}$)
Ni_{100} 600	**437**	**39.4**
Co_{100} 600	**151**	**96.19**
$Ni_{90}Co_{10}$ 600	**536**	**54.28**
$Ni_{80}Co_{20}$ 600	**451**	**60.06**
$Ni_{70}Co_{30}$ 600	**515**	**83.92**
(*) $Ni_{60}Co_{40}$ 600	**566**	**94**
$Ni_{50}Co_{50}$ 600	**150**	**143**

(*) $Ni_{60}Co_{40}$ 600 shows stability 84% up to 10000 cycles

Table S5 : XPS peak positions of Co(2p), Ni(2p) & O(1s) in $Ni_{60}Co_{40}$ 600 after 10000 GCD cycles.

Elements	Binding Energy	Inferences
Co	781.1eV($2p_{3/2}$) and 796.6 eV($2p_{1/2}$)	**Co^{+2}**
	780eV($2p_{3/2}$) and 795 eV($2p_{1/2}$)	**Co^{+3}**
	790.1eV (satellite) and 804.8eV(satellite)	**Co^{+3}**
Ni	855.7eV($2p_{3/2}$) and 873.3eV($2p_{1/2}$) 861.5eV(satellite) and 879.8 eV(satellite)	**Ni^{+3}**
O	532.7eV	**adsorbed water**
	531.1eV	**Lattice O**
	529.3eV	**O^{2-} formation**

Table S6: ICP-AES analysis Cobalt (Co), Nickel(Ni) and phosphorous (P) concentrations in the as prepared $Ni_{60}Co_{40}$ 600, after it's electrochemical activation (after 200 cycle), after stability

Sample id	P amount (ppm)
$Ni_{60}Co_{40}$ 600 (as prepared)	**8.698**
$Ni_{60}Co_{40}$ 600 after precondition (after 200 CV cycles)	**1.045**
$Ni_{60}Co_{40}$ 600 after Stability (after 10000 GCD cycles)	**0.872**

Table S7: Comparison of cyclic Stability values reported for different pyrophosphate-based supercapacitor electrode materials in 3 electrode system with the result obtained from the present study.

SL No	Electrode material	Synthesis of precursor	Electrode Substrate	Stability (%)	Specific Capacitance/ Capacity	Reference
1.	Na Doped $Ni_2P_2O_7$	Hydrothermal	Ni foam	97.3% (1000 cycles)	557 Fg^{-1} at (at 1.2Ag^{-1})	2
2.	Co_3O_4-C/$Ni_2P_2O_7$ composite	Hydrothermal	Ni foam	88.5% (3000 cycles)	2,537.78 Fg^{-1} (at 2Ag^{-1})	3
3.	Na doped $Ni_2P_2O_7$-$Co_2P_2O_7$	Hydrothermal	Ni foam	*98.8%* (2000 cycles)	295 Cg-1 (at 2Ag^{-1})	4
4.	$Zn_2P_2O_7$	hydrothermal	Ni foam	81.58 % (1000 cycles)	102.9Fg^{-1} (at 1Ag^{-1})	5
5.	$Co_2P_2O_7$ with redox additive $K_3Fe(CN)_6$	hydrothermal	Carbon paper	96% (5000 cycles)	580Fg^{-1} (at 1Ag^{-1})	6
6.	$Cu_2P_2O_7$	hydrothermal	Ni foam	94.04 % (1000 cycles)	297.5Fg^{-1} (at 1Ag^{-1})	7

7.	$Co_2P_2O_7$	Calcination followed by co precipitation	Ni foam	90 % (3000 cycles)	483Fg^{-1} (at 1Ag^{-1})	[8]
8.	$Ni_2P_2O_7$ (CTAB)	Chemical precipitation	Graphitic foil	-	250Fg^{-1} (at 2Ag^{-1})	[9]
9.	**$Ni_{60}Co_{40}$ 600**	**Co-precipitation**	**Carbon paper**	**94%(up to 5000 cycles) & 84% (up to 10000 cycles)**	**566 Fg^{-1} at (at 1Ag^{-1})**	**This work**

Table S8: Comparison of cyclic stability values reported for different pyrophosphate-based hybrid capacitors in a two-electrode system with the corresponding results from the present study.

SL no	**Electrode material**	**Substrate**	**Stability (%)**	**Voltage window**	**Power density (Wkg^{-1}) & Energy density ($Whkg^{-1}$)**	**Reference**
1.	Na Doped $Ni_2P_2O_7$ //graphene	Ni foam	98.5% (5000 cycles)	0 - 1 V	23.4$Whkg^{-1}$ at 1292.2Wkg^{-1}	[2]
2.	$Cu_2P_2O_7$//$Cu_2P_2O_7$	Stainless steel	85% (4500 cycles)	0 - 0.9 V	11.54$Whkg^{-1}$ at 2760Wkg^{-1}	[10]
3.	$Ni_2P_2O_7$ (CTAB) // CTAB	Graphitic foil	70% (4500 cycles)	0 - 1.6 V	23$Whkg^{-1}$ at 775Wkg^{-1}	[9]
4.	$Co_2P_2O_7$@N–C_2//AC	Ni foam	76.7% (10000 cycles)	0 - 1.3V	5.68$Whkg^{-1}$at 325Wkg^{-1}	[11]
5.	**$Ni_{60}Co_{40}$ 600//AC**	**Carbon paper**	**87% (up to 25000 cycle)**	**0 - 1.6 V**	**14.9 $Whkg^{-1}$ at 794 Wkg^{-1}**	**This work**

References:

(1) M. Haghani and S. Daneshpazhuh, *J. Environ. Anal. Chem.,* 2020**, 7**, 273.

(2) C. Wei, C. Cheng, S. Wang, Y. Xu, J. Wang and H. Pang, *Chem. - An Asian J.,* 2015, **10**, 1731–1737.

(3) Y. Zhou, X. Li, J. Li, S. Yin, D. Shen, C. Li, P. Huo, H. Wang, Y. Yan and S. Yuan, *Chem. Eng. J.,* 2019, **378**, 122242.

(4) C. Wei, S. Yang, W. Liu, X. Hou, Y. Sun, J. Zhao, W. Xiong, C. Cheng and D. Zhan, *Appl. Surf. Sci.,* 2019, **465**, 763–771.

(5) A. Karaphun, S. Sawadsitang, T. Duangchuen, P. Chirawatkul, T. Putjuso, P. Kumnorkaew, S. Maensiri and E. Swatsitang*, Surfaces and Interfaces,* 2021, **23** , 100961.

(6) Z. Khan, B. Senthilkumar, S. Lim, R. Shanker, Y. Kim and H. Ko, *Adv. Mater. Interfaces,* 2017. **4** , 1700059.

(7) A. Karaphun, P. Chirawatkul, S. Maensiri and E. Swatsitang, *J. Sol-Gel Sci. Technol.,* 2018, **88**, 407–421.

(8) L. Hou, L. Lian, D. Li, J. Lin, G. Pan, L. Zhang, X. Zhang, Q. Zhang and C. Yuan, *RSC Adv.,* 2013, **3** (44), 21558–21562.

(9) M. Priyadharshini, M. Sandhiya, M. Sathish, T. Pazhanivel, G. Mani, A. A. Alothman and K. N. Alqahtani*, J. Mater. Sci. Mater. Electron.,* 2022, **33**, 9269–9276.

(10) A. Agarwal and B. R. Sankapal, *Chem. Eng. J.,* 2021, **422**, 130131.

(11) H. Aydın, Ü. Kurtan, B. Üstün and S. N. Koç, *Mater. Chem. Phys.,* 2022, ***290*,**126392.